Archive of SID.ir

*Journal of Applied Fluid Mechanics*, Vol. 14, No. 4, pp. 1137-1146, 2021.
Available online at www.jafmonline.net, ISSN 1735-3572, EISSN 1735-3645.
https://doi.org/10.47176/jafm.14.04.32243

# Experimental and Numerical Investigation of Flow in Hydraulic Elbows

Y. Selim Korkmaz[1], A. Kibar[2†] and K. Suleyman Yigit[3]

[1] *Altan Hydraulic Engineering Industry and Trade Corporation, Istanbul, 34956, Turkey*
[2] *Department of Mechanical and Material Technologies, Kocaeli University, Uzunciftlik Nuh Cimento Campus, 41180, Kocaeli, Turkey*
[3] *Department of Mechanical Engineering, Kocaeli University, Umuttepe Campus, 41380, Kocaeli, Turkey*

†*Corresponding Author Email: alikibar@kocaeli.edu.tr*

(Received September 24, 2020; accepted January 10, 2021)

## ABSTRACT

Elbow fittings are common in hydraulic and pipeline systems. These components cause a significant pressure drop in the total pressure of a system. The banjo elbow is advantageous in areas low to the ground and where flexible connection angles are needed. However, this elbow yields a larger pressure drop than a standard elbow. Additionally, the position of the internal bolt in the banjo elbow cannot be determined prior to installation, which corresponds to a wide range of possible pressure drop. In this study, the pressure drop through a 3/8" banjo elbow is investigated for different positions of the internal bolt, experimentally and numerically. Experiments and simulations were carried out on hydraulic oil with four different Reynolds numbers ranging from 3111 to 6222 and at nine bolt connection angles ranging from 0° to 60°. Experiments were repeated with the standard elbow of the same size to compare the pressure drops to those of the banjo elbow. Pressure was measured at both the inlets and outlets of the elbows. The results suggest that the connection angle of the internal bolt is an important factor in the pressure drop and minor head loss through a banjo elbow. For Reynolds numbers of 3111 and 6222, an improvement in minor head loss by 33% and 58%, respectively, was achieved by adjusting the connection angle of the internal bolt in the banjo elbows.

**Keywords**: Hydraulic, Minor loss; Pressure prop; Banjo elbow; Numerical study.

## 1. INTRODUCTION

Hydraulic systems are used in a wide range of industrial applications, such as construction machinery, heavy industrial machinery, defense industry vehicles, trucks, and buses. As a result of the development of technology and increased competition, engineers are working to reduce costs. One effective approach to reducing cost is to increase efficiency. The lack of free space in a system or machine poses a significant problem, leading designers to design smaller alternative components.

The main factor affecting efficiency in hydraulic systems is the pressure drop (or loss). The pressure drop decreases available energy. A component that is applied unnecessarily or incorrectly may cause an avoidable pressure drop in the hydraulic system. In this case, for example, a bigger pump is required to provide enough pressure in the system, clearly increasing energy costs.

Pressure loss, in particular, influences pipe design. It is critical to investigate the pressure drop through the fittings in most pipeline systems, as the pressure drops through fittings are higher than in straight pipe with similar properties (Beutner and Rumsey 2006).

When the liquid or gas flows in pipes or ducts, a pressure drop (or head loss) occurs owing to the friction. Calculating the head loss in a pipe system is crucial because the pump power requirement is a function of pressure loss. There are two types of head losses in hydraulic systems including in major and minor. While major head loss is due to friction of the liquid along the pipe, minor loss (or dynamic pressure loss) arises from the momentum change of the liquid.

In the case of fully-developed internal flow, Eq. (1) can be used to express the major head loss as the Darcy-Weisbach equation in pressure loss form ($\Delta P$):

$$\Delta P = f \frac{L}{D} \frac{\rho V^2}{2} \tag{1}$$

where $f$, $L$, $\rho$, $D$, and $V$ are the Darcy friction factor, length of pipe, density of the liquid, hydraulic

Archive of SID.ir

Archive of SID.ir



diameter of the pipe, and mean velocity of the liquid, respectively.

Minor loss forms in components, such as elbows, bends, and valves that change in the direction or velocity of the flow. Therefore, minor head loss occurs under the following conditions: sudden contraction/expansion, entrance/exit of a pipe, obstruction in a pipe, bend in a pipe, and various fittings (Yunus and Cimbala 2006). These components interrupt the flow and cause losses owing to the mixing and flow separations. Minor losses are determined using the minor loss coefficient $K_L$ and can be calculated from Eq. (2):

$$h_L = K_L \frac{V^2}{2g} \tag{2}$$

where $g$ is the acceleration due to gravity and $h_L$ is the additional irreversible head loss in the piping system caused by insertion of the component, defined by Eq. (3):

$$h_L = \frac{\Delta P}{\rho g} \tag{3}$$

where $\Delta P$ is the pressure difference between the inlet and outlet of the component.

The minor loss coefficient depends on the pressure drop, velocity, and density and can be expressed by Eq. (2) with Eq. (3), as given in Eq. (4):

$$\Delta P = K_L \rho \frac{V^2}{2} \tag{4}$$

Fittings with diameter and shape changes, such as valves, elbows, T-junctions, contractions, and expansions, are mostly used in hydraulic and pipeline system installation. They are essential in controlling flow rate, changing flow direction, etc. The change in velocity and direction of the flow causes energy losses in the systems (Perumal and Ganesan 2016). A small reduction in pressure loss can decrease energy consumption and increase efficiency in the hydraulic system. Efficiency can significantly improve by reducing the pressure losses caused by liquid flowing in pipes and components. High pressure drop requires more pressure to perform the desired work. Furthermore, the pressure drop causes additional heat to be produced in the system, which must be removed properly (Zardin *et al.* 2017).

Bends and elbows provide convenience in hydraulic system design. A pipeline system typically contains one or more of these components. The elbow orientation of a standard elbow cannot be adjusted. Standard elbows are also difficult to install in tight spaces. In such cases, banjo elbows are preferred. These fittings can easily be installed in small spaces and allow for direction adjustment after installation. This is achieved with a banjo bolt, which can rotate independently inside the body. Because banjo elbows are advantageous in these respects compared to standard elbows, they are used in many applications, such as brake systems in the automotive industry, diesel engines, agricultural equipment, air conditioning systems, and construction equipment. However, one disadvantage of the banjo elbow is that it results in a much higher pressure loss compared to a standard elbow. In the present study, these differences are evaluated by experimental and numerical analyses.

Alternatively, swivel elbows can be installed to allow movement during operation (see Fig. 2). Banjo elbows provide rotational flexibility during the assembly but, then remain fixed. Swivel elbows allow rotation to prevent the hose from twisting and kinking during operation. However, they have disadvantages such as friction, less rigidity, and high cost due to the internal rotating parts.

Many studies have investigated the flow in pipeline systems. These works can be classified as straight pipe (Kitoh 1991), bends at different angles (Valsala *et al.* 2019; Röhrig *et al.* 2015; Liu *et al.* 2019; Rinaldi *et al.* 2019), elbow (Zahedi *et al.* 2019), T-junctions (Štigler *et al.* 2012), manifold (Zardin *et al.* 2017; Zhang *et al.* 2019) valve (Okhotnikov *et al.* 2020; Lisowski and Rajda 2013) etc. Valsala *et al.* 2019 studied the flow characteristics in a tube with a 90° bend, examining the effects of vane number and shape on pressure loss. Specific vane count and fin shape reduce the secondary flows and thus reduce the pressure losses. Murakami *et al.* (1969) examined an experimental study about the flow in the commercial elbows, comparing the head loss and flow characteristics of a single elbow and two elbows. Okhotnikov *et al.* (2020) performed an experimental and numerical study of a rotary tubular spool inside a valve. Flow and pressure losses in the valve, according to the angular positions of the spool, were investigated in their study. Zardin *et al.* (2017) examined the pressure losses and flow in hydraulic manifolds and also studied the effect of the angular position of the spool. Zhang *et al.* (2019) investigated the pressure loss under different conditions with various geometry properties and suggested that pressure loss can be significantly reduced by up to 50% by adopting a smooth transition. To the best of our knowledge, an analysis of flow and pressure drop through the banjo elbow has yet to be performed prior to the present study.

Most industrial hydraulic flow systems with high flow rates are not purely single-phase. Many researchers have recently explored pressure drop with low-to-medium-void fractions for two-phase bubbly flow in pipes, bends and other hydraulic fittings (Spedding and Bénard 2007; Ma *et al.* 2015; Tryggvason *et al.* 2016; Kim *et al.* 2010; Ma *et al.* 2016).

The minor pressure loss that occurs in pipeline systems is due to flow separation, secondary flow, and swirling of the flow, results in pressure drop and energy loss. These events consume energy that cannot be converted to useful work. They cause an increase in the viscous heating and unused force to the body.

The position of the internal bolt has a significant effect on the pressure drop through a banjo elbow. Unfortunately, the position of this internal bolt



Archive of SID.ir

Archive of SID.ir



cannot be known prior to installation. Therefore, the location of it is left to chance, corresponding to a wide range of possible pressure drop coefficients.

In this study, the flow behaviour and pressure drop as functions of the position of the internal bolt are investigated across a banjo elbow. The potential pressure drops at various Reynolds numbers are evaluated. For this purpose, both experimental and numerical studies are performed. A detailed analysis can be difficult through an experimental setup. Therefore, the numerical results are first validated through experimental data and then a detailed analysis of the flow phenomena is performed using numerical results.

In the present study, experimental and numerical results are used primarily to investigate the flow phenomenon. Fractal modification can be adapted to examine pressure drop in detail using theoretical study since the flow boundary is unsmooth because of internal bolt (see Zhao *et al*. 2009; Wang and Deng 2019; Yang *et al*. 2020).

## 2. Experimental Materials and Methods

In this study, both experimental and numerical studies were carried out to examine flow and pressure drop in banjo and standard elbows. In the experiments, pressure drops in the banjo elbows were investigated for different flowrates. Experimental results validated the numerical results. Thus, flow parameters, such as velocity and pressure, in the banjo elbow could be studied in detail using the numerical results.

### 2.1 Experimental Studies

Figure 1 shows the experimental setup used in this study. In this setup, the flowrate capability ranged from 0 to 300 lpm, measured by a Webtec flowmeter (CT300-SR-B-B-6with accuracy ± 1% of indicated reading). All experiments used ISO VG 22 hydraulic oil for the working fluid.

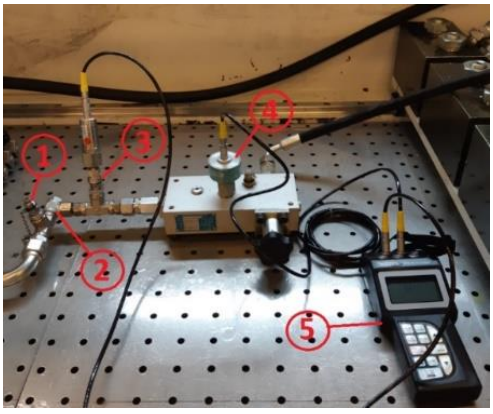


**Fig. 1. Experimental setup. 1-Connector for outlet pressure, 2-Banjo elbow, 3-Connector for inlet pressure, 4-Flowmeter, 5-Datalogger.**

Physical properties of this oil are shown in Table 1. The pump rotation speed was controlled by a driver such that the desired flow rate could easily be adjusted. Oil temperature and pressure sensor (SR-PTT-600-05-0C in range from 0 to 600 bar with an accuracy 0,25% of full scale) were measured during the experiments. All data (temperature, pressure and flowrate) were recorded by the Webtec (SR-HPM-460-05-0C) datalogger, as shown in Fig. 1.

**Table 1 Physical properties of ISO VG 22 hydraulic oil.**

| Property | Value |
|---|---|
| Kinematic viscosity | 22 cST |
| Temperature | 40 °C |
| Density | 860 kg/m³ |

The standard and British Standard Pipe (BSP) banjo elbows (3/8” thread), which are common fittings in industry, were used in this experiment (see Fig. 2).


**Fig. 2. Fittings used in the experiments, 3/8” standard (left) swivel (middle) and 3/8” banjo elbows (right).**

Figure 3 shows the geometry of the banjo elbow having a total length of 50.80 mm. The diameter of the banjo body is 27.40 mm. There are three holes in this component 120° apart with an elliptical shape (major axis of 4.5 mm, minor axis of 3.5 mm) and at a 45° angle with respect to the bolt axis, as shown in Fig. 3b. The incoming liquid enters the bolt through the three holes after which the three flows combine, having changed the flow direction by 90°, as shown in Fig. 3c.

The temperature of the oil was heated to 40 °C, accepted the optimum value in hydraulic systems, before starting the experiments. The oil was kept at this temperature throughout the experiments to avoid any change in viscosity. Four different flow rates, 30, 40, 50 and 60 lpm were tested to determine pressure drop. Since pressure drops at flow rates below 30 lpm (Re=3111) were low, these test conditions weren't included in this study. Nine different positions (connection angles) of the internal bolt were tested, ranging from 0° to 60°, as shown in Fig. 4. The internal bolt was rotated by 7.5° for each experiment. Flow behaviours at angles between 0° and 60° and between 60° and 120° were determined to be symmetrical. This comparison was repeated three times after 120° connection angle of bolt up to 360° (i.e. 0−120°, 120−240°, 240−360°). Therefore, the experiments could be limited to connection angles between 0° and 60°.



Archive of SID.ir

Archive of SID.ir



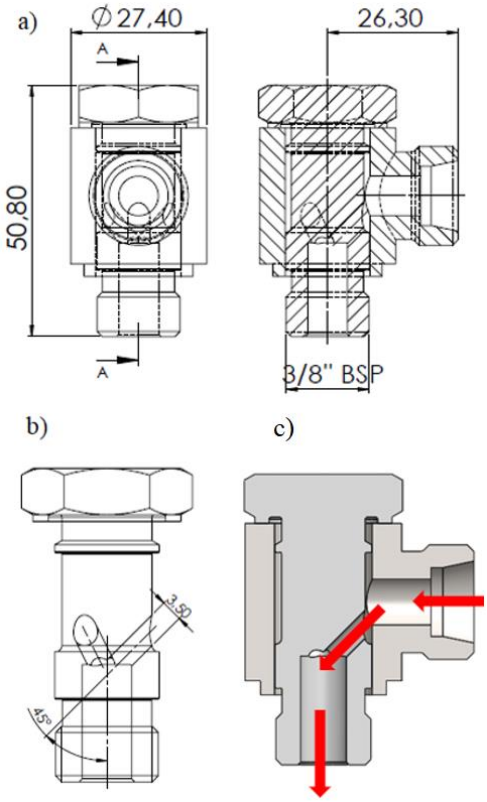


**Fig. 3. Banjo elbow section view and flow direction, a) dimensions, b) diameter and angle of holes, and c) direction of the flow.**

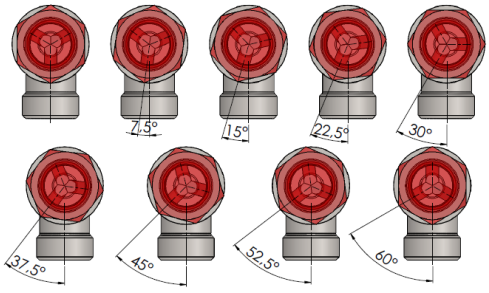


**Fig. 4. Positions of the internal bolt (red) in the banjo elbow.**

## 3. NUMERICAL METHOD AND MODELLING

The 3D simulation of the flow was performed using the commercial CFD code Star CCM+. The behaviour of the flow was determined by solving Navier-Stokes equations with steady-state conditions. The SIMPLE algorithm was adopted for pressure-velocity coupling, and the QUICK scheme was used for the momentum equation. The realisable *k-ε* turbulence model was chosen to simulate flow since this model was successfully applied in similar studies. For example, Kim *et al.* (2014) studied different turbulence models for the numerical analysis of flow in an elbow. The *k-ε* turbulence model yielded more accurate results for primary streamwise velocity and secondary flow than the other turbulence models. Dutta *et al.* (2016) also suggested this model for both single and two-phase flows in a pipe bend.

The governing equations of the flow simulations are the mass and momentum conservation equations. The mass conservation equation is as follows:

$$\frac{\partial \rho}{\partial t} + \nabla.\left(\rho \vec{V}\right) = 0 \tag{5}$$

where $\vec{V}$ and $\rho$ are the velocity vector and density of the liquid, respectively. In incompressible flow, $\rho$ is constant, and, therefore, $\partial\rho/\partial t=0$. Hence, the mass conversion equation can be described as $\nabla\cdot\vec{V}=0$.

The momentum conservation equation is as follows:

$$\frac{\partial \vec{V}}{\partial t} + \nabla.\left(\rho \vec{V}\vec{V}\right) = \vec{f_b} - \nabla p + \nabla.\tau \tag{6}$$

where $p$ and $\vec{f_b}$ are the static pressure and the resultant of the body forces (e.g. gravitational and centrifugal forces), respectively. $\tau$ is the viscous stress tensor for Newtonian fluids, as described in Eq. (7):

$$\tau = \mu\left[\left(\nabla\vec{V} + \nabla\vec{V}^T\right) - \frac{2}{3}\nabla.\vec{V}I\right] \tag{7}$$

where $I$ and $\mu$ are the unit tensor and dynamic viscosity of the liquid, respectively. The second term in the Eq. (7), is the effect of volume dilation. The Star CCM+ solved all governing equations with the finite-volume method.

### 3.1. Geometric Model and Boundary Conditions

Figure 5a shows the 3D model of the banjo elbow, which has two parts, the banjo body and the internal bolt, shown as an exploded assembly in Fig. 5c. The computational domain (shown in blue in Fig. 5b) was obtained by intersecting the interval volumes of the banjo body and internal bolt. Other domains were created by rotating the internal bolt 7.5° to obtain different connection angles. Thus, nine different 3D domains were used to examine the flow phenomena at each flow rate with respect to the connection angle in this study. In total, 36 domains were analysed for four flow rates and nine connection angles.

Pressure sensors were connected to the banjo elbow's entrance and exit with tee-junctions (see Fig. 1) using nipples. To determine the pressure drop across these fittings, simulations were performed with and without the fittings. The increase in pressure drop from the fittings was considered insignificant compared to the overall pressure drop in the banjo elbow. Therefore, this effect was neglected in the simulations.

Figures 6a and 6b show the geometric model of the 3D simulation for 0° and 60° internal bolt connection angles, respectively. Nine geometrical models with bolt angles of 0.0, 7.5, 15.0, 22.5, 30.0, 37.5, 45.0, 52.5 and 60.0° were analysed to determine the effect of the internal bolt position on pressure drop.



Archive of SID.ir

Archive of SID.ir



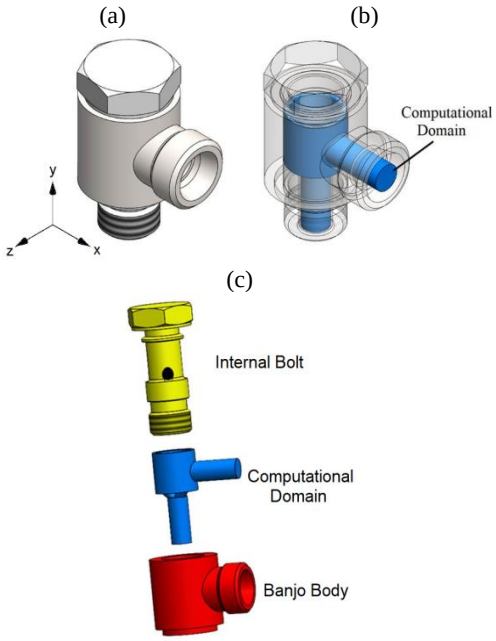


**Fig. 5. (a) 3D CAD model, (b) computational domain, and c) exploded assembly of the banjo elbow.**

The liquid enters the banjo elbow at its inner diameter of 8 mm, then flows among the coaxial cylinders with diameters of 13.65 and 17.10 mm before flowing through the three elliptical holes, and finally exits at the same diameter of 8 mm, as illustrated in Fig. 6a.

Mass flow inlet and pressure outlet (0 Pa) boundary conditions were applied to simulate the flow, as shown in Fig. 6b. The environmental approach was used for the pressure boundary to discourage backflow from occurring. All walls were defined as wall boundaries with no-slip and adiabatic boundary conditions.

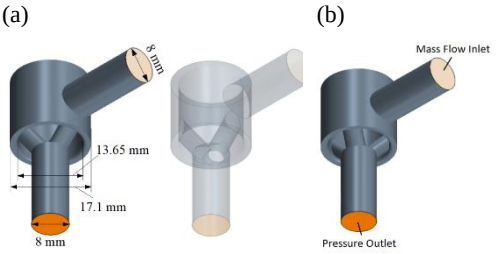


**Fig. 6. (a) 3D Geometrical model of the simulation with an internal bolt angle of 0° and b) boundary conditions for the internal bolt angle of 60°.**

### 3.2. Mesh Domain and Mesh Independence Study

In this study, a tetrahedral mesh was used in the flow simulation through the banjo elbow, as shown in Fig. 7. In similar studies with curved surfaces, tetrahedral meshing has yielded good results. Five different mesh structures were created to ensure that the solution is independent of mesh. Table 2 shows the exact total number of cells, approximately 150 000, 300 000, 500 000, 1 000 000, and 2 500 000, for these five cases.

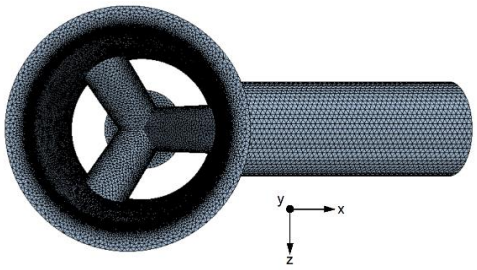


**Fig. 7. Tetrahedral mesh structure of the banjo elbow.**

**Table 2 Mesh cell numbers of structures created for mesh independence.**

| Case | Number of mesh cells |
|---|---|
| Case 1 | 147966 |
| Case 2 | 308 936 |
| Case 3 | 505 358 |
| Case 4 | 1 037 865 |
| Case 5 | 2 487 752 |

The pressure drop occurring between the inlet and outlet of the banjo elbow, which is the most important output of the study, is the basis for the mesh independence study. For this purpose, the pressure drops of the five mesh cases and the experimental results were used for validation of the simulations as shown in Fig. 8. The pressure drops obtained using Case 1 and Case 2 are smaller than experimental results. Pressure drop is almost not affected by the number of meshes after Case 3. which has the lowest sufficient number of elements and most closely matches the experimental results. Since there were a total of 36 simulations to be run in this study, Case 3 was found sufficient to evaluate the simulated results with the experimental results while minimising processing time.

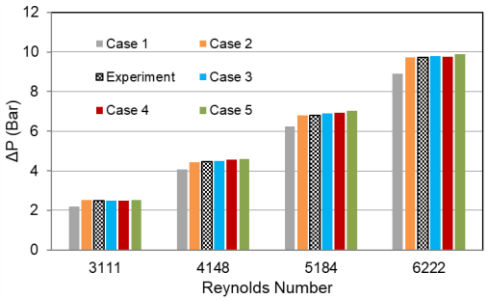


**Fig. 8. Pressure loss dependent on the mesh size for mesh independence study.**

The convergence criterion of each residual was determined as $10^{-5}$ for all the governing parameters. The enhanced wall treatment function was employed to control the non-dimensional distance ($y^+$) from the



Archive of SID.ir

Archive of SID.ir



wall (Eq. 8). The wall-adjacent cells were refined to provide wall function of $y^+ \approx 1$ and higher $y^+ < 3$ in the present study.

$$y^+ = \frac{yu^*}{\upsilon} \tag{8}$$

where $y$, $u^*$ and $v$ are the normal distance from the wall, reference velocity and kinematic viscosity, respectively.

## 4. RESULTS AND DISCUSSION

In this study, both experimental and numerical studies are carried out to examine the pressure drop across the banjo elbow. Figure 9 shows the pressure drop with respect to the connection angle at different flow rates. The numerical simulation results agree well with the experimental results.

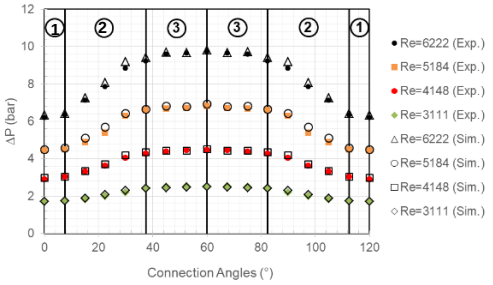


**Fig. 9. Pressure drops of the banjo elbow with respect to the connection angles.**

The connection angle of the internal bolt does not have a significant effect on the pressure drop with Reynolds numbers in the range of 0 to 3111. The pressure drop is lowest when the bolt connection angle is 0°. It is 1.70, 2.97, 4.49 and 6.32 bar in the cases of Reynolds numbers equal to 3111, 4148, 5184, and 6222, respectively. The pressure drop increases with Reynolds number, as shown in Fig. 9, and rises as the connection angle increases from 0° reaching a maximum value at 60°. While the pressure drop difference between 0° and 60° connection angles is approximately 0.70 bar for Re=3111, it approaches 3.60 bar for Re=6222.

The pressure drop behaves in three different ways according to the bolt connection angle, which range from 0.0−7.5°, 7.5−37.5°, and 37.5−60.0°. While the pressure drop increases only slightly between 0.0−7.5° connection angles (section 1 in Fig. 9), it increases at the fastest rate between 7.5 and 37.5° angles (section 2). The rate slows down significantly with connection angles larger than 37.5°, and the pressure drop reaches a maximum value at the 60° connection angle (section 3). The connection angle of the internal bolt is symmetrical with respect to 0−60° and 60−120°. This symmetrical behaviour repeats every 120° up to 360°. In the case of Re=6222, although a pressure difference of 2.89 bar is occurred between 7.5−37.5° connection angles, a pressure difference of 0.49 bar is occurred between 37.5−60.0° angles. These results suggest that while there is an acceptable pressure drop between 0.0° and 7.5° connection angles, the pressure drop increases significantly for connection angles greater than 7.5°. Thus, for a low pressure drop, the connection angle should be connected with a ±7.5° tolerance for each hole of the internal bolt. These are 352.5−7.5°, 112.5−127.5°, and 232.5−247.5° connection angles.

Figure 10 shows the minor loss coefficient, which is obtained from Eq. (4), for the banjo and standard elbows. Both coefficients do not change considerably with the Reynolds numbers. The minor loss coefficient occurring in Banjo elbow with a 0° bolt connection angle is roughly 1.5 times more than that of the standard elbow. This difference increases as the bolt connection angle increases and maximises, 2.3 times larger than the standard elbow, at a 60° connection angle. Therefore, in the cases of Reynolds numbers of 3111 and 6222, the minor head loss can improve by 33% and 58%, respectively, by adjusting the connection angle of the internal bolt for a banjo elbow.

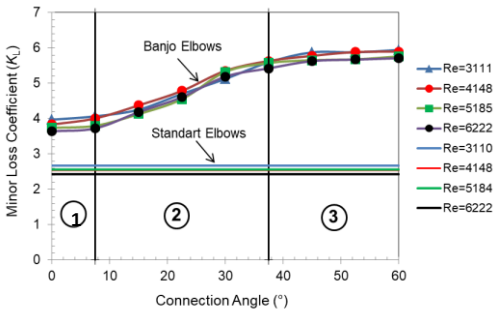


**Fig. 10. Minor loss coefficients for standard and banjo elbows.**

The behaviour of the minor loss coefficient in a Banjo elbow can be examined in three connection angle ranges, 0.0−7.5°, 7.5−37.5°, and 37.5−60°, as labelled in Fig. 10. In the first range, or part 1, the inlet section of the liquid is aligned with the hole in the internal bolt at the 0° connection angle, as shown in Fig. 11. The inlet begins to misalign as the bolt connection angle increases. Nevertheless, both holes overlap, even if they are not fully aligned, up to approximately 37.5° bolt connection angle, as shown in Fig. 11.

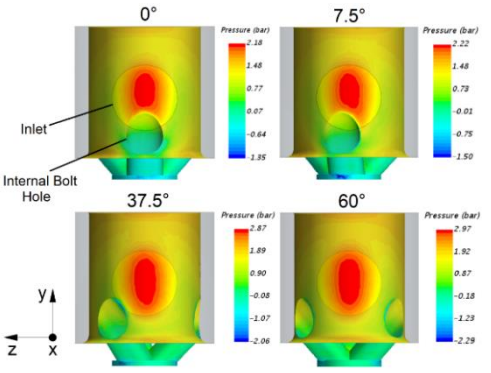


**Fig. 11. Pressure distribution on the internal bolt hole at different connection angles (Re=3111).**



Archive of SID.ir

Archive of SID.ir



**Table 3 Probabilities of the pressure drop for the different parts shown in Fig. 10.**

| | Part 1 | Part 2 | Part 3 |
|---|---|---|---|
| Possibilities (%) | 12.5% | 50.0% | 37.5% |
| Connection angles ranges (°) | 352.5°–7.5°<br>112.5°–132.5°<br>232.5°–252.5° | 7.5°–37.5°<br>82.5°–112.5°<br>127.5°–157.5°<br>202.5°–232.5°<br>247.5°–277.5°<br>322.5°–252.5° | 37.5°–82.5°<br>157.5°–202.5°<br>277.5°–302.5° |
| Connection angles (°) | 45°/360° | 180°/360° | 135°/360° |

In the range of 0.0−7.5°, the minor loss coefficient increases slightly. In the range of 7.5−37.5° connection angle, the minor loss coefficient increases significantly as the bolt connection angle increases. This happens as the holes misalign. In the range of 37.5−60.0° connection angle, the alignment between the bolt hole and the inlet vanishes completely, as shown in Fig. 11. In this case, the incoming liquid hits the bolt wall directly and flows around the bolt to enter through the holes. At angles larger than 37.5°, the minor loss coefficient changes slightly. The maximum pressure increases with an increase in the connection angle on the internal bolt, as seen in Fig. 11, as does the magnitude of the negative pressure.

The connection angle of the internal bolt cannot be determined prior to or known subsequently after installation of the banjo elbow to the pipeline. Thus, the pressure drop also cannot be known and is left to chance. Table 3 shows the probability of the bolt connection angle corresponding to the three parts shown in Fig. 10. The internal bolt may result in any connection angle after installations. While the best connection angles of the bolt in terms of pressure drop are in part 1, the worst angle is in part 3. Installing the fitting according to part 3 is three times more likely than part 1. The probability of part 2, which has a much broader spectrum than the other two parts, is 50%. In conclusion, there is a substantial chance of having the maximum pressure drop in banjo elbow applications. Providing the internal bolt coincides with one of the angle positions in part 1, it will be of great benefit in terms of energy loss. Marking the bolt with three arrows to indicate the three holes can be an intelligent solution to obtain minimal pressure drop for these applications.

Figure 12 shows flow, shown as streamlines, around the internal bolt. In the case of the 0° bolt connection angle, one of the three holes of the bolt is aligned with the inlet (region A, as shown in Fig. 12c). Thus, region A located at the bottom of the incoming liquid enters the bolt directly through this hole, as shown in Fig. 12a. The incoming liquid in region C first contacts the bolt wall and then is directed downwards before entering this hole. The incoming liquid in region B also enters this same hole by making a 360° loop after hitting the internal bolt wall. The liquid coming from region D wraps around the bolt and enters the two holes on the sides. A small amount of

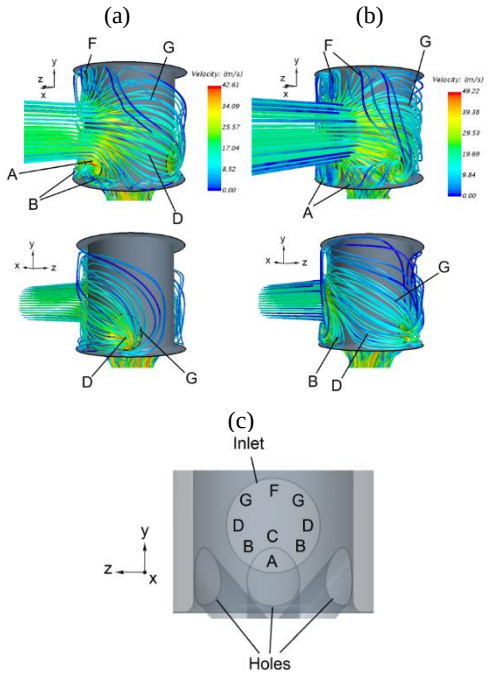


**Fig. 12. Flow around the internal bolt inside the banjo elbow, (a) 0° bolt connection angle, Re=6222, (b) 60° bolt connection angle, Re=6222, and c) Regions of the inlet.**

incoming liquid in region F forms the vortices in the upper part of the banjo elbow and is then directed to the holes on either side. The incoming liquid in the region G crosses upward after hitting the bolt wall. Then it flows downward and enters the two side holes. The incoming liquid in both regions D and G, which enters the holes on both sides in different directions and speeds, forms a small number of vortices.

In the case of the 60° internal bolt angle, incoming liquid hits the internal bolt wall directly before spreading around the bolt. The incoming liquid in region A is directed towards the bottom, forming many vortices. This vortex-shaped flow enters in both holes on the sides. The incoming liquid in region B also goes around the internal bolt and enters these two holes at high speed. The liquid in the region F section is directed towards the upper side and forms vortices here. Then, it is directed to the sides and enters the side holes at low speed. Liquids coming from region A, B, and F enter both side holes



Archive of SID.ir

Archive of SID.ir



at different speeds and directions, resulting in a large number of vortices. Liquids coming from region D and G also flow around the internal bolt and enter the hole in the opposite direction of the inlet. The maximum velocity of the liquid occurs at the entrance to this hole since the incoming liquid regions D and G are directed to both sides, combine, and enter this hole.

Figure 13 shows the vortices and separation of the flow in the case of the 60° bolt connection angle. Liquid coming from regions A, B and F form a large number of vortices as they enter both side holes. Although the incoming liquid in region B enters these holes at a high velocity, the incoming liquid in regions A and F flows by forming vortices and enters these holes with lower velocity. Since these flows enter the holes from the inlet flow direction, a large amount of flow separation occurs in this area, as shown in Fig. 13.

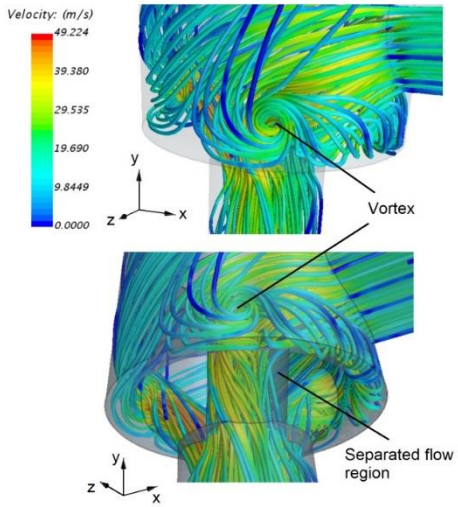


**Fig. 13. Liquid entering the holes and creating vortices, 60° bolt connection angle, Re=6222.**

Figure 14 shows the velocity at a mid-plane section of the banjo elbow. The liquid enters the front hole directly in the case of the 0° bolt connection angle. The maximum velocity of the flow occurs in this section, as shown in Fig. 14a. Since the inlet and bolt holes are not coaxial, the liquid enters the bolt hole's upper side at maximum speed. This results in flow separation between the upper and lower regions of the bolt hole. This event is similar for the 60° bolt connection angle. In this case, the liquid enters the holes after wrapping around the bolt. Figure 14b shows the velocity of liquid entering the hole opposite to the inlet, as a scalar scene at mid-plane. The liquid, which combines after wrapping on both sides of the bolt, enters in the bolt through this hole. The inlet velocity of the liquid is higher for this case than the 0° connection angle case. The liquid enters in the hole at a smaller angle than the 45° hole angle at a high velocity. Therefore, flow separation occurs in the flow field in this region, as shown in Fig. 14b. This part of the liquid, which enters in the bolt through three different holes, then combines again before the exit. The velocities of these three flows are different. Flow separation occurs on the side of the hole where the maximum velocity is, as shown in Figs. 14a and 14b.

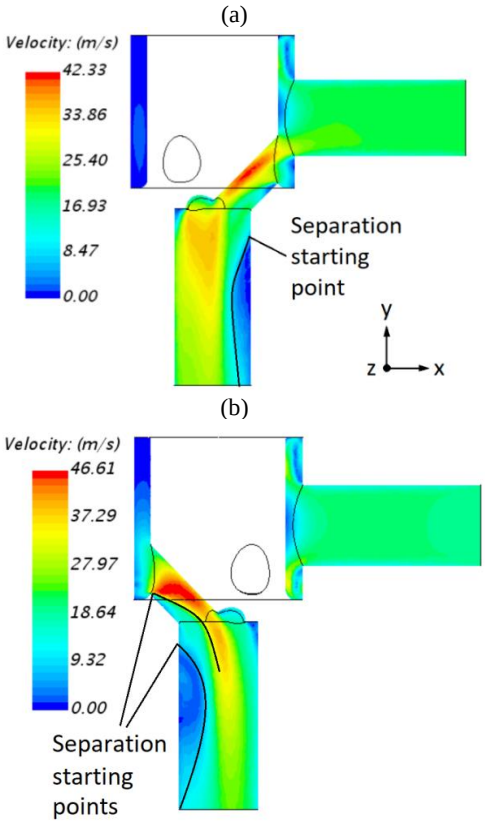


**Fig. 14. Velocity at the mid-plane. 60° bolt connection angle, Re=6222.**

The flow event is very complex especially between the combined flow and outlet sections, as shown in Fig. 15. In the case of the 0° connection angle, the flow is symmetrical. Therefore, the combining of flow after passing through the holes behaves symmetrically. Vortices with different forms arise during the flow, as shown in Fig. 15. Dean vortices also appear in Fig. 15, as evident on the bends. Two counter-rotating vortices are caused by swirling motion of flow (Valsala *et al.* 2019). The vortices, dean vortices or swirl-switching flow, occur because of the secondary flow perpendicular to the main flow direction (Noorani and Schlatter 2016). The unsteady motion is due to these flow types (Noorani and Schlatter 2016). The vortices show different behaviours at different bolt connection angles, as shown in Fig. 15.

## 5. CONCLUSION

The pressure drop occurring in the banjo elbow is more significant than in the standard elbow. At the same time, the banjo elbow exhibits a wide range of pressure drops depending on the connection angle of its internal bolt. Nevertheless, the exact pressure drop cannot be determined because the bolt



Archive of SID.ir

Archive of SID.ir



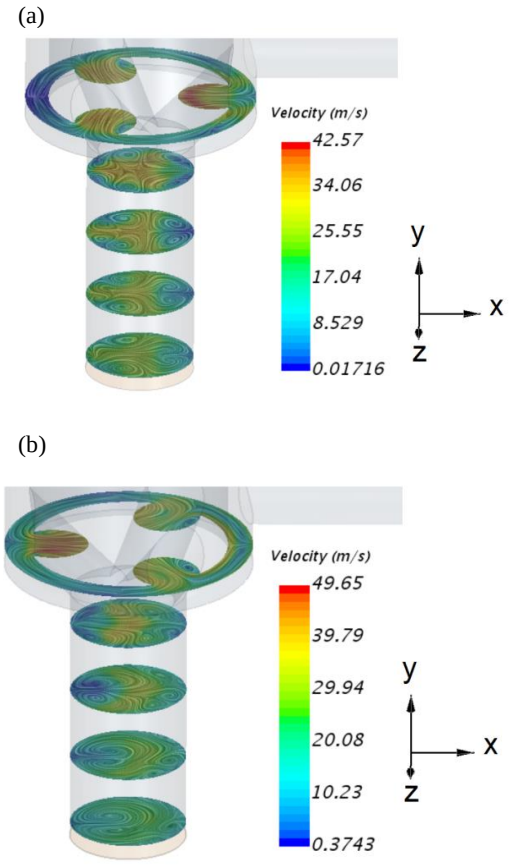


**Fig. 15. Velocity at various planes. a) 0° and b) 60° bolt connection angles, Re=6222.**

connection angle with respect to the holes directions on the bolt is unknown. This study suggests that the adjustment of the connection angle is an essential factor in reducing energy consumption by lowering the pressure drop.

For a system with a flow rate of 60 lpm (Re=6222), the 0° connection angle, the best case, produces 58% of the pressure drop produced by the 60° connection angle, which is the worst case. This percentage decreases as the Reynolds number decreases, 33% for the case of 30 lpm (Re=3111).

The pressure drop between the banjo elbow is approximately 1.5 times that of the standard elbow for the best cases (0°, 120°, and 240°) and 2.3 times for the worst cases (60°, 180°, and 300°).

A banjo elbow is a very practical fitting for small spaces. However, its pressure drop is higher than the standard elbow. If the connection angle of the internal bolt is not considered, this difference may be significant.

## REFERENCES

Beutner, T. and C. Rumsey (2006). Introduction: Computational fluid dynamics validation for synthetic jets. *AIAA Journal* 44(2), 193-193.

Dutta, P., S. K. Saha, N. Nandi and N. Pal (2016). Numerical study on flow separation in 90 pipe bend under high Reynolds number by k-ε modelling. *Engineering Science and Technology, an International Journal* 19(2), 904-910.

Kim, J., M. Yadav and S. Kim (2014). Characteristics of secondary flow induced by 90-degree elbow in turbulent pipe flow. *Engineering Applications of Computational Fluid Mechanics* 8(2), 229-239.

Kim, S., G. Kojasoy and T. Guo (2010). Two-phase minor loss in horizontal bubbly flow with elbows: 45 and 90 Elbows. *Nuclear Engineering and Design* 240(2), 284-289.

Kitoh, O. (1991). Experimental study of turbulent swirling flow in a straight pipe. *Journal of Fluid Mechanics* 225, 445-479.

Lisowski, E. and J. Rajda (2013). CFD analysis of pressure loss during flow by hydraulic directional control valve constructed from logic valves. *Energy Conversion and Management* 65, 285-291.

Liu, C., D. Yu, W. Akram, Y. Cai and X. Chen (2019). Ratcheting behavior of pressurized elbow pipe at intrados under different loading paths. *Thin-Walled Structures* 138, 293-301.

Ma, M., J. Lu and G. Tryggvason (2015). Using statistical learning to close two-fluid multiphase flow equations for a simple bubbly system. *Physics of Fluids* 27(9), 092101.

Ma, M., J. Lu and G. Tryggvason (2016). Using statistical learning to close two-fluid multiphase flow equations for bubbly flows in vertical channels. *International Journal of Multiphase Flow* 85, 336-347.

Murakami, M., Y. Shimizu and H. Shiragami (1969). Studies on fluid flow in three-dimensional bend conduits. *Bulletin of JSME*, 12(54), 1369-1379.

Noorani, A. and P. Schlatter (2016). Swirl-switching phenomenon in turbulent flow through toroidal pipes. *International Journal of Heat and Fluid Flow* 61, 108-116.

Okhotnikov, I., K. Abuowda, S. Noroozi and P. Godfrey (2020). Numerical and experimental investigation of the metering characteristic and pressure losses of the rotary tubular spool valve. *Flow Measurement and Instrumentation* 71, 101679.

Perumal, K. and R. Ganesan (2016). CFD modeling for the estimation of pressure loss coefficients of pipe fittings: An undergraduate project. *Computer Applications in Engineering Education* 24(2), 180-185.

Rinaldi, E., J. Canton and P. Schlatter (2019). The vanishing of strong turbulent fronts in bent pipes. *arXiv preprint arXiv*:1902.02294.

Röhrig, R., S. Jakirlić and C. Tropea (2015). Comparative computational study of turbulent flow in a 90 pipe elbow. *International Journal of Heat and Fluid Flow* 55, 120-131.



Archive of SID.ir

Archive of SID.ir



Spedding, P. L. and E. Bénard (2007). Gas–liquid two phase flow through a vertical 90 elbow bend. *Experimental Thermal and Fluid Science* 31(7), 761-769.

Štigler, J., R. Klas, M. Kotek and V. Kopecký (2012). The Fluid Flow in the T-Junction. The Comparison of the Numerical Modeling and PIV Measurement. *Procedia Engineering* 39, 19-27.

Tryggvason, G., M. Ma and J. Lu (2016). DNS–assisted modeling of bubbly flows in vertical channels. *Nuclear Science and Engineering* 184(3), 312-320.

Valsala, R. R., S. W. Son, A. Suryan and H. D. Kim (2019). Study on reduction in pressure losses in pipe bends using guide vanes. *Journal of Visualization* 22(4), 795-807.

Wang, Y. and Q. Deng (2019). Fractal derivative model for tsunami traveling. *Fractals* 27(02), 1950017.

Yang, Z., Z. Li, D. Feng, J. Li, W. Wan, T. Yu, L.Y. Xu, X. Yao, J. Cao and X. Feng (2020). A fractal model for pressure drop through a cigarette filter. *Thermal Science* 24(4), 2653-2659.

Yunus, A, C. and M. Cimbala John (2006). *Fluid Mechanics, Fundamental and Application*.

Zahedi, P., M. Parsi, A. Asgharpour, B. S. McLaury and S. A. Shirazi (2019). Experimental investigation of sand particle erosion in a 90° elbow in annular two-phase flows. *Wear*, 438, p.203048.

Zardin, B., G. Cillo, C. A. Rinaldini, E. Mattarelli and M. Borghi (2017). Pressure losses in hydraulic manifolds. *Energies* 10(3), 310.

Zhang, J. H., G. Liu, R. Ding, K. Zhang, M. Pan and S. Liu (2019). 3D printing for energy-saving: evidence from hydraulic manifolds design. *Energies* 12(13), 2462.

Zhao, L., G. C. Wu and J. H. He (2009). Fractal approach to flow through porous material. *International Journal of Nonlinear Sciences and Numerical Simulation* 10(7), 897-902.



Archive of SID.ir